Romanian Reports in Physics, Vol. 57, No. 4, P. 889–903, 2005

CAN SOLITARY WAVES FORM IN A LITHIUM TRIBORATE OPTICAL PARAMETRIC OSCILLATOR?

L.-C. CRASOVAN[1], D. MIHALACHE[1], R. ILIEW[2], C. ETRICH[2], F. LEDERER[2]

[1] *Department of Theoretical Physics,*
Horia Hulubei National Institute of Physics and Nuclear Engineering,
Institute of Atomic Physics, PO Box MG-6, Bucharest, Romania and
[2] *Institute of Solid State Theory and Theoretical Optics,*
Friedrich-Schiller-University Jena, Max-Wien-Platz 1, D-07743, Germany

(Received June 8, 2005)

Abstract. We investigate the possibility of solitary wave formation in a singly resonant synchronously pumped lithium triborate based optical parametric oscillator for both femtosecond and picosecond pump pulses. The influence of the cavity parameters, pump irradiance, crystal length and desynchronization between pump and resonated wave on the solitary wave formation is investigated in detail. In the femtosecond regime, for a wide range of pump durations, the width of the solitary wave formed in the cavity is inverse proportional to the pump amplitude when pumping the cavity with the same energy. Stable femtosecond pulses have been shown to emanate from the optical parametric oscillator even at small anomalous and normal signal dispersions. In the picosecond pumped cavity, for moderate peak power, a 5-fold compression may be achieved.

Key words: solitary waves, lithium triborate, optical oscillators, femtosecond range.

1. INTRODUCTION

In the past decade both the emergence of new nonlinear crystals and the introduction of advanced laser pump sources, in particular all-solid-state and ultrashort-pulse devices, have evoked a renaissance in the practical realization of optical parametric oscillators (OPO's) and optical parametric generators providing coherent light in all time scales, from the ultrafast femtosecond to the continuous-wave (cw) operating regimes, and covering the electromagnetic spectrum from the near-ultraviolet deep into the mid-infrared (for excellent reviews, see [1–4] and the references therein). By using periodically poled materials such as lithium niobate ($LiNbO_3$) or potassium titanyl phosphate ($KTiOPO_4$) and by applying intracavity and pump-enhancement techniques cw OPO's with commonly available low- to moderate-power sources have been implemented. [5–7] Recently realized cw watt-level OPO's are currently finding a burgeoning range of applications in spectroscopy, medical diagnostics and therapy, atmospheric optics, environmental monitoring

and optical communications. On the other hand, synchronously pumped OPO's have established themselves as practical sources for femtosecond and picosecond pulses at high repetition-rates, covering spectral regions from the visible to the mid infrared, often from a single device. They are now recognized as important tools in time-resolved spectroscopy of semiconductors, in confocal microscopy as well as in infrared imaging. A great deal of attention has been attracted to materials that can be periodically poled and allow thus for quasi phase matching, such as $LiNbO_3$, $LiTaO_3$, $KTiOPO_4$ and $RbTiOAsO_4$ [8–14]. Worthy to mention are also compression effects reported in femtosecond and picosecond pumped parametric devices [13–21]. Other recent theoretical and experimental studies concentrated on the optical properties of the new nonlinear material BiB_3O_6 (bismuth borate) for efficient high-average-power second harmonic generation of femtosecond pulses into the blue spectral region [22].

In view of this wide field of potential applications for OPO's with ultrashort pulses at the output it is worthwhile to address the question of stable intra-cavity pulse (or solitary wave) formation. This aspect has been only marginally addressed in the literature, from both the experimental [23] and theoretical [24] viewpoint. In Ref. [24] it has been shown that in a singly resonant cavity just above threshold the signal pulse can be described by a cubic-quintic Ginzburg-Landau equation having solitary wave solutions. Moreover, it was argued that stable soliton formation requires the presence of a stabilizing third-order nonlinearity.

The aim of this paper is to investigate in detail solitary-wave formation in a lithium triborate (LBO) based singly-resonant synchronously pumped OPO. LBO is a very promising nonlinear material because of its high optical damage threshold (about 10 GW/cm^2), broad transparency window (0.16–2.5μm), anomalous group-velocity dispersion (GVD) in a wide frequency range and temperature-tuned noncritical phase-matching (NCPM) capability [25–33]. Particular emphasis will be paid to the influence of pump pulse width, peak power, energy, crystal length and desynchronization on the solitary-wave formation process. The role of the third-order nonlinearity and the sign of GVD will be also studied. The paper is organized as follows: In Section 2 we briefly characterize the unique properties of the LBO crystal and present the geometry used. Section 3 contains the results of the extensive numerical experiments showing the solitary-wave formation in the LBO crystal. The results of this work are briefly summarized in Section 4.

2. MODEL EQUATIONS AND MATERIAL PARAMETERS

We deal here with an OPO, formed by a LBO crystal placed in a cavity. The input pump enters the cavity and, through the parametric process taking place in the nonlinear quadratic crystal, generates signal and idler waves. The relation

between the frequencies of the three waves is: $\omega_p = \omega_s + \omega_i$, where ω_p, ω_s and ω_i are the pump, signal and idler frequencies, respectively. One can tune the output frequency (signal and idler) between infrared and ultraviolet. The LBO crystal is a birefringent one belonging to the orthorhombic system with point symmetry $mm2$. The type-I NCPM condition for an "eoo"-configuration [27, 32] reads as: $k_p^e = k_s^o + k_i^o$, where k_p, k_s and k_i are the pump, signal and idler wavenumbers, respectively. Here the superscripts "o" and "e" stand for "ordinary-wave" and "extraordinary-wave", respectively.

Our aim is to investigate in detail the possibility of solitary-wave formation by using singly resonant cavities [24]. The pump enters the cavity and one of the wave generated inside the LBO crystal is in resonance and remains in the cavity. In what follows this wave is termed *signal* wave. We consider here the case when the signal is synchronized with the pump at the entrance of the crystal. The cavity consists of two mirrors which are perfectly transparent for pump and idler, one of them reflects the entire signal, the other one having a reflection coefficient less than unity.

The LBO nonlinear crystal exhibits both quadratic and cubic optical nonlinearities [31]. Bearing in mind that only the signal wave is resonant with the cavity it suffices to take into account only self-phase modulation, evoked by third-order nonlinear effects, of this wave. Cross-phase modulation is generally neglected in our model.

The equations that describe the parametric process in the nonlinear crystal are:

$$i\frac{\partial A_s}{\partial z} + ik_s'\frac{\partial A_s}{\partial t} - \frac{1}{2}k_s''\frac{\partial^2 A_s}{\partial t^2} - \frac{i}{6}k_s'''\frac{\partial^3 A_s}{\partial t^3} + \Gamma_s A_p A_i^* + k_s n_2 |A_s|^2 A_s = 0 \tag{1}$$

$$i\frac{\partial A_p}{\partial z} + ik_p'\frac{\partial A_p}{\partial t} - \frac{1}{2}k_p''\frac{\partial^2 A_p}{\partial t^2} - \frac{i}{6}k_s'''\frac{\partial^3 A_p}{\partial t^3} + \Gamma_p A_s A_i = 0 \tag{2}$$

$$i\frac{\partial A_i}{\partial z} + ik_i'\frac{\partial A_i}{\partial t} - \frac{1}{2}k_i''\frac{\partial^2 A_i}{\partial t^2} - \frac{i}{6}k_i'''\frac{\partial^3 A_i}{\partial t^3} + \Gamma_i A_p A_s^* = 0 \tag{3}$$

where, A_s, A_p and A_i are the slowly-varying envelopes of the signal, pump and idler electric fields, respectively, k_s, k_p and k_i are their wavenumbers, and the primes denote derivatives with respect to the frequency. The Γ's are the second order nonlinear coefficients and n_2 is the intensity-dependent refractive index coefficient. We have taken $n_2 = 3\times10^{-20}$ m^2/W [24, 31]. The second order nonlinear coefficients are given by:

$$\Gamma_{s,p,i} = \frac{2\pi d_{eff}}{\lambda_{s,i,p}}\left(\frac{2}{c\varepsilon_0 n_s n_i n_p}\right)^{1/2}$$

and are measured in $W^{-1/2}$. Here d_{eff} is a phase-matched effective second order coefficient, $\lambda_{s,i,p}$ and $n_{s,i,p}$ are the signal, idler and pump wavelengths and refractive indices, respectively. For LBO a typical value of d_{eff} is 1.25 pm/V. The electric fields $A_{s,i,p}$ in equations (1)–(3) are expressed in $W^{1/2}/m$, so that the quantities $\left|A_{s,i,p}\right|^2$ give us the signal, idler and pump intensities in W/m^2. The normalized equations, appropriate for the numerical scheme we have developed, read as

$$i\frac{\partial u}{\partial Z}-\frac{1}{2}d_2^s\frac{\partial^2 u}{\partial T^2}-\frac{i}{6}d_3^s\frac{\partial^3 u}{\partial T^3}+vw^*+\theta|u|^2u=0 \tag{4}$$

$$i\frac{\partial v}{\partial Z}+i\delta_p\frac{\partial v}{\partial T}-\frac{1}{2}d_2^p\frac{\partial^2 v}{\partial T^2}-\frac{i}{6}d_3^p\frac{\partial^3 v}{\partial T^3}+2uw=0 \tag{5}$$

$$i\frac{\partial w}{\partial z}+i\delta_i\frac{\partial w}{\partial T}-\frac{1}{2}d_2^i\frac{\partial^2 w}{\partial T^2}-\frac{i}{6}d_3^i\frac{\partial^3 w}{\partial T^3}+vu^*=0 \tag{6}$$

where

$$T=\frac{t-k_s'z}{\tau_0},\quad Z=\frac{z}{z_0},\quad v=A_pz_0\left(\Gamma_s\Gamma_i\right)^{1/2},$$

$$w=A_iz_0\left(\frac{\Gamma_s\Gamma_p}{2}\right)^{1/2},\quad u=A_sz_0\left(\frac{\Gamma_p\Gamma_i}{2}\right)^{1/2}$$

$$\delta_{p,i}=(k_{p,i}'-k_s')\frac{z_0}{\tau_0},\quad d_2^{s,p,i}=k_{s,p,i}''\frac{z_0}{\tau_0^2},\quad d_3^{s,p,i}=k_{s,p,i}'''\frac{z_0}{\tau_0^3},\quad \theta=\frac{4\pi n_2}{\lambda_s\Gamma_p\Gamma_iz_0}$$

and τ_0 and z_0 being the time and propagation scales, respectively. We have chosen the time scale $\tau_0 = 100$ fs, and the length scale $z_0 = 25$ mm. In almost all of our simulations the crystal length was assumed to be $L = 2.5$ mm.

As mentioned above LBO is a birefringent crystal. We have used Eq. (2) from Ref. [29] (the so called Sellmeier's equations) for expressing the principal refractive indices as a function of the wavelength. Their dependence on the temperature have been taken from experimental data reported in the literature [30].

Fig. 1(a) presents the temperature dependence of the generated wavelengths in a type-I NCPM configuration for three different pump wavelengths. The curves we got correspond very well to the experimentally measured ones [25–28]. The temperature dependences of the GVD's for the pump and the generated waves are plotted in Fig. 1(b). This plot was traced for a pump wavelength of 760 nm. We will use this pump wavelength in all our calculations. Point "O" in Fig. 1(b) corresponds to zero GVD. Notice that the pump and one of the generated waves always exhibit normal and anomalous GVD, respectively, whereas the third wave

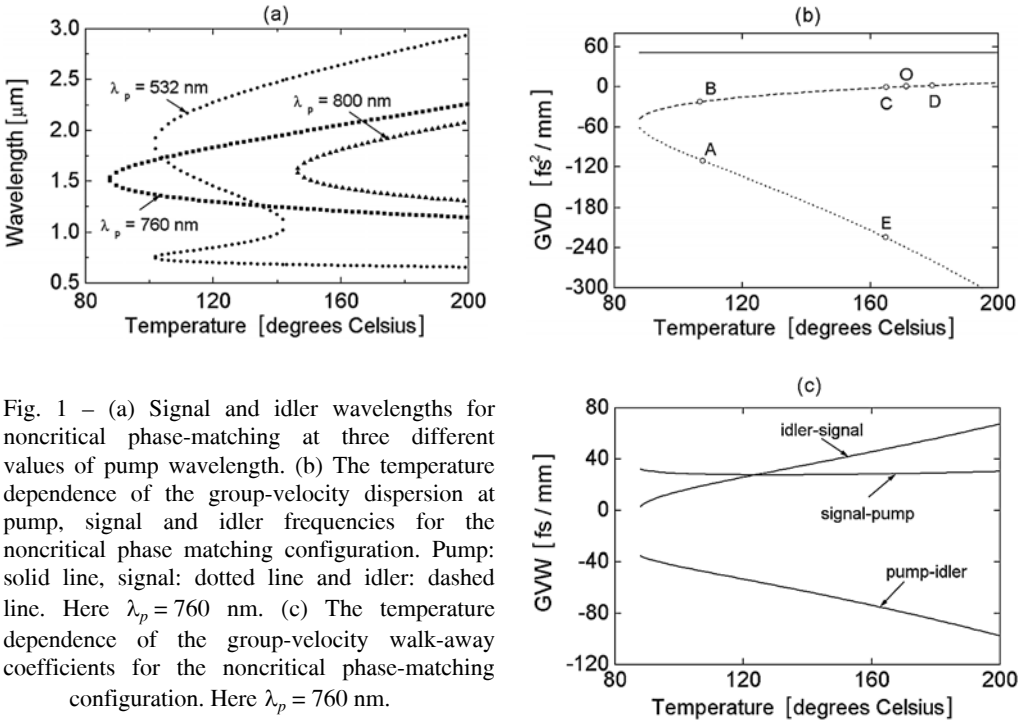

Fig. 1 – (a) Signal and idler wavelengths for noncritical phase-matching at three different values of pump wavelength. (b) The temperature dependence of the group-velocity dispersion at pump, signal and idler frequencies for the noncritical phase matching configuration. Pump: solid line, signal: dotted line and idler: dashed line. Here $\lambda_p = 760$ nm. (c) The temperature dependence of the group-velocity walk-away coefficients for the noncritical phase-matching configuration. Here $\lambda_p = 760$ nm.

has, depending on the temperature, regions of normal and anomalous GVD. Other important quantities are the group-velocity walk-away (GVW) coefficients defined as: $\Delta_{s,p} = k'_s - k'_p$, $\Delta_{p,i} = k'_p - k'_i$, $\Delta_{i,s} = k'_i - k'_s$. Their temperature dependence for a 760 nm pump is shown in Fig. 1(c).

3. NUMERICAL EXPERIMENTS

In this section we present and discuss the results of our intensive numerical calculations. We have solved equations (4)–(6) for each pass through the crystal. The numerical scheme used is based on the split-step algorithm. Typical values of the longitudinal step $h_z = 0.001$ and of the transverse step $h_t = 0.03$ that assure an energy conservation with an acuracy of 10^{-3} were used. Upon reflection at the mirror the signal field u becomes Ru, R being the field reflection coefficient. We have used input Gaussian pumps: $v = v_0 \exp\left(-T^2/t_0^2\right)$ in all the investigated cases. For a time scale $\tau_0 = 100$ fs, $t_0 = 1$ corresponds to a pulse with an intensity full-width at half maximum (FWHM) of approximately 120 fs. In the majority of our simulations we have taken $t_0 = 1$ (corresponding thus to 120 fs pump pulses). Throughout the paper we have explicitly indicated the cases when the simulations

were performed with pump durations different from that value. A normalized pump amplitude $v_0 = 5$ corresponds to an irradiance of approximately 0.8 GW/cm^2.

A typical solitary wave formation at the temperature $t = 107$°C, *i.e.* for point A in Fig. 1(b), needs approximately 200 round trips. As expected, solitary-wave formation may occur only for pump irradiances above a threshold value. We have numerically identified the threshold pump irradiance for 120 fs input pulses for two typical reflectivities: $I_{th} = 0.24$ GW/cm^2 for $R = 0.99$, and $I_{th} = 0.55$ GW/cm^2 for $R = 0.96$, showing the expected increase in threshold pump irradiance with the decrease in mirror reflectivity. In Fig. 2 we compare the build-up time, the shape and the chirp of the solitary waves emerging from the OPO for two different input pump irradiances.

For small irradiances (about 3 times above the threshold value) the signal chirp is only slightly different (see the dashed line in Fig. 2(c)) from that resulting from the associated cubic-quintic complex Ginzburg-Landau equation describing the solitons of singly resonant OPO [24]. For large input pump irradiances (about

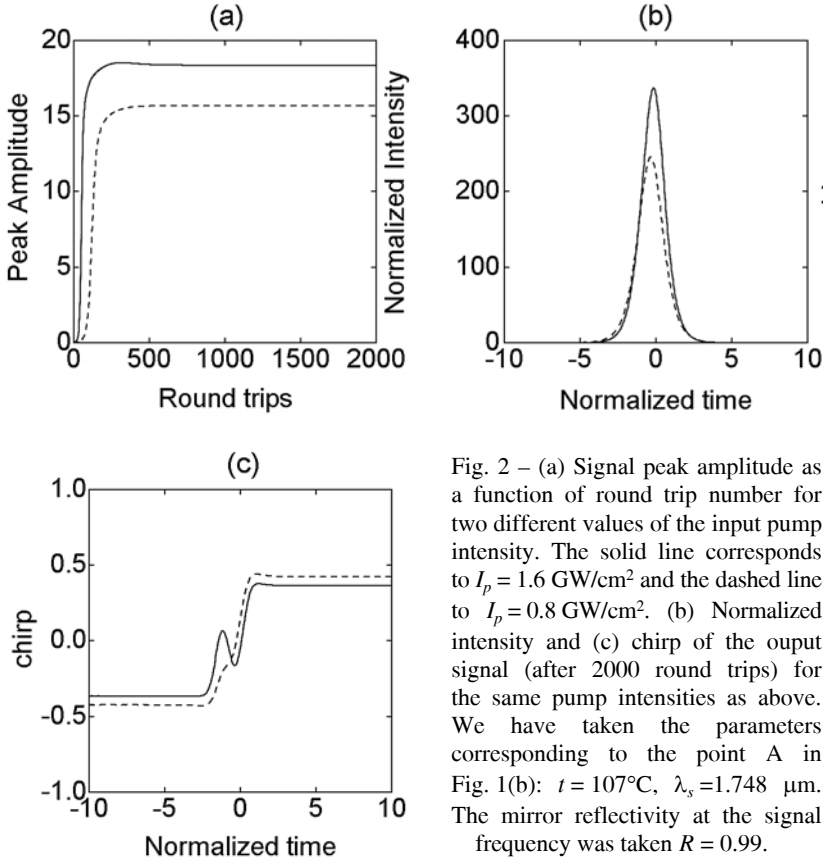

Fig. 2 – (a) Signal peak amplitude as a function of round trip number for two different values of the input pump intensity. The solid line corresponds to $I_p = 1.6$ GW/cm^2 and the dashed line to $I_p = 0.8$ GW/cm^2. (b) Normalized intensity and (c) chirp of the ouput signal (after 2000 round trips) for the same pump intensities as above. We have taken the parameters corresponding to the point A in Fig. 1(b): $t = 107$°C, $\lambda_s = 1.748$ μm. The mirror reflectivity at the signal frequency was taken $R = 0.99$.

6 times above threshold) the signal chirp displays a rather complicate behavior (see the solid line in Fig. 2(c)).

The mirror reflection coefficient at the signal frequency is a key parameter in OPO experiments. Our simulations indicate that the greater the reflection coefficient the stronger will be the output signal. Fig. 3 compares two typical situations differing only in the value of the reflection coefficient. Notice that, in this case, the build-up time practically does not depend on the radiation losses.

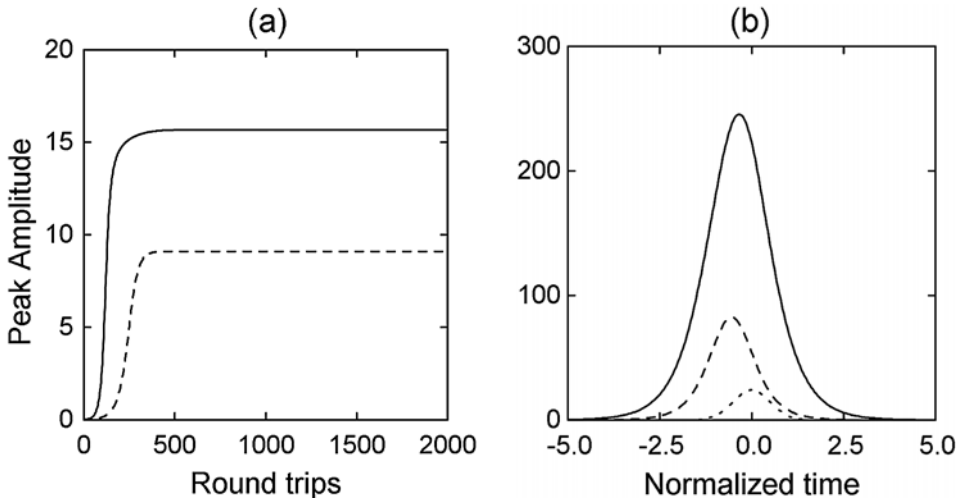

Fig. 3 – (a) Signal peak amplitude as a function of round trip number for two values of the mirror reflectivity. The input pump intensity is $I_p = 0.8$ GW/cm^2. (b) Normalized intensity of the ouput signal (after 2000 round trips). The dotted line corresponds to the pump intensity profile. In both figures the solid lines correspond to $R = 0.99$ and the dashed lines to $R = 0.96$. We have taken the parameters corresponding to the point A in Fig. 1(b).

One important issue related to singly resonant OPO's is the influence of the input pump duration on the emerging signal. In order to study this issue we have kept the pump intensity constant and performed simulations for different pump durations, between 300 fs and 2 ps. The corresponding output intensity profiles, after 2000 round-trips are presented in Fig. 4(a). The signal pulses displayed here reach the stationary regime after less than 1000 round trips. A significant compression coefficient (see Fig. 4(b)), defined as the FWHM ratio of the pump and the generated signal may be achieved. For this pump irradiance and for pump durations larger than 1.1 ps the signal wave displays pronounced shoulders, showing thus that the pump energy exceeds the necessary energy for single-soliton formation. By decreasing the input pump irradiance to $I_p = 0.3$ GW/cm^2, and by increasing the pump duration to 4 ps, we have obtained a 5-fold compression (see Fig. 5), *i.e.*, 800 fs signal output pulses, a bit smaller than those reported for other nonlinear crystals, [13, 16–20] due to a smaller nonlinearity of LBO and the geometry used in our simulations.

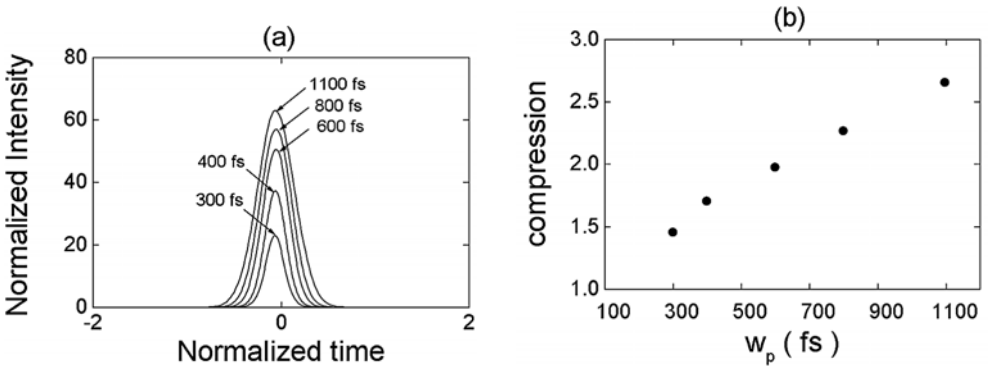

Fig. 4 – (a) Signal intensity profile for different pump durations, indicated with the arrows. Here $I_p = 0.4$ GW/cm^2, the reflectivity $R = 0.96$, and the other parameters correspond to the point A in Fig. 1(b). (b) Compression coefficient *versus* pump duration for the same parameters as above.

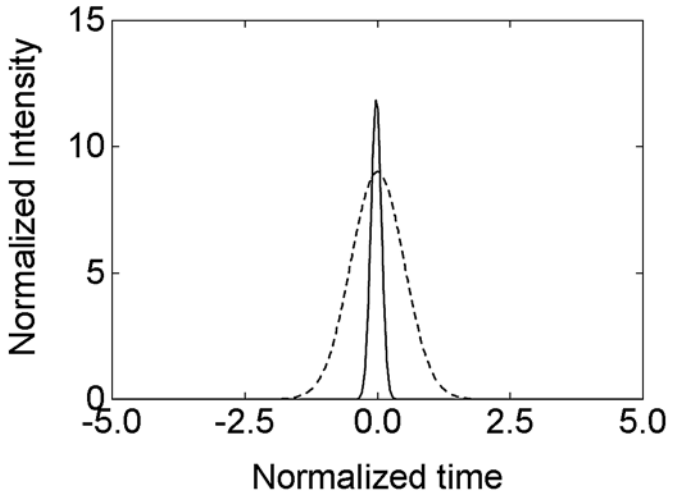

Fig. 5 – Intensity profile *versus* normalized time. Full line: Signal after 10000 round-trips, dashed line: 4 ps input pump. The parameters correspond to the point A in Fig. 1(b). Here $I_p = 0.3$ GW/cm^2, and $R = 0.96$.

For a better characterization of the resonated solitary wave we have varied the pump durations by keeping constant the pump energy. The outcomes of our calculations are shown in Fig. 6. For pump pulses between 100 fs and 500 fs the quantity $A_p \times w_s$, where A_p is the pump amplitude and w_s is the signal FWHM, is constant with 1% accuracy. This is an indication that the pulse formed in the femtosecond pumped OPO is a solitary wave, not a trivial chirped pulse, sustaining thus our nomenclature. For larger pump durations this law ceases to hold.

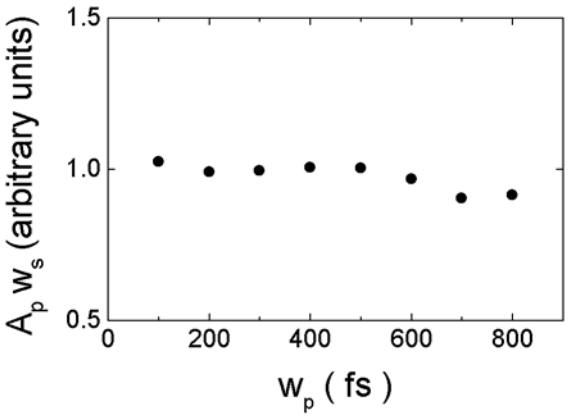

Fig. 6 – Pump amplitude A_p times signal width w_s *versus* pump duration for a constant pump energy.

A major question one may raise is whether the solitary waves form even in the vicinity of the zero GVD point O in Fig. 1(b). Concerning this issue we have performed calculations with parameters corresponding to point C in Fig. 1(b) (slightly before point O) and with parameters corresponding to the point D (slightly after point O) in the same figure, that is, in the normal dispersion regime. Our results, presented in Fig. 7, reveal that soliton formation is possible even for these material parameters, in agreement with previous experimental results which demonstrated the formation of temporal solitons near zero GVD of an ultrafast

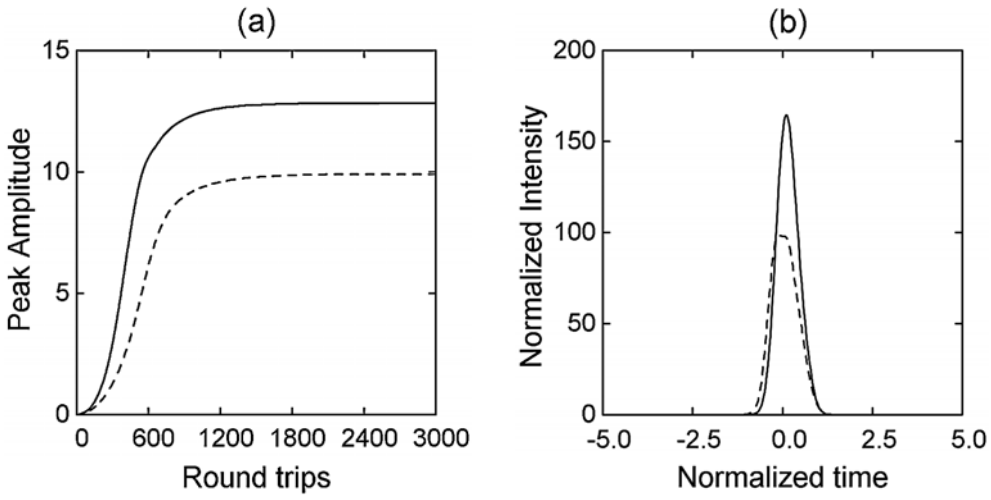

Fig. 7 – (a) Signal peak-amplitude as a function of round trip number for two different temperatures, slightly before (point C in Fig. 1(b)) and slightly after (point D in Fig. 1(b)) the zero group-velocity dispersion point O in Fig. 1(b). (b) Normalized intensity of the output signal (after 3000 round trips) for the two cases considered above. The solid lines stand for $t = 165$°C, $\lambda_s = 1.198$ μm (point C in Fig. 1(b)), while the dashed lines for $t = 180$°C, $\lambda_s = 1.173$ μm (point D in Fig. 1(b)). The input pump intensity is $I_p = 0.8$ GW/cm^2, and the reflectivity $R = 0.982$.

OPO [23]. The intensity profile of the output solitons is of a typical "triangular" shape. Similar "triangular-like" pulses were shown to occur in a simplified LBO-based OPO model [34]. One can observe that a stabilization of these output pulses occur only after 1000 round trips, as a consequence of the presence of a small positive GVD.

The signal build-up time for large negative GVD is shorter than the corresponding build-up time for a small negative GVD (see Fig. 8(a)). In accordance with the above results, the shape of the emerging signal at temperature $t = 165°C$ in the region of small negative GVD (point C in Fig. 1(b)) is a "triangular-like" one, while the signal shape in the region of large negative GVD (point E in Fig. 1(b) is a "sech-like" one (see Fig. 8(b)). Thus, one can perform pulse shaping, by keeping in the cavity one wave or its companion from the two parametrically generated waves.

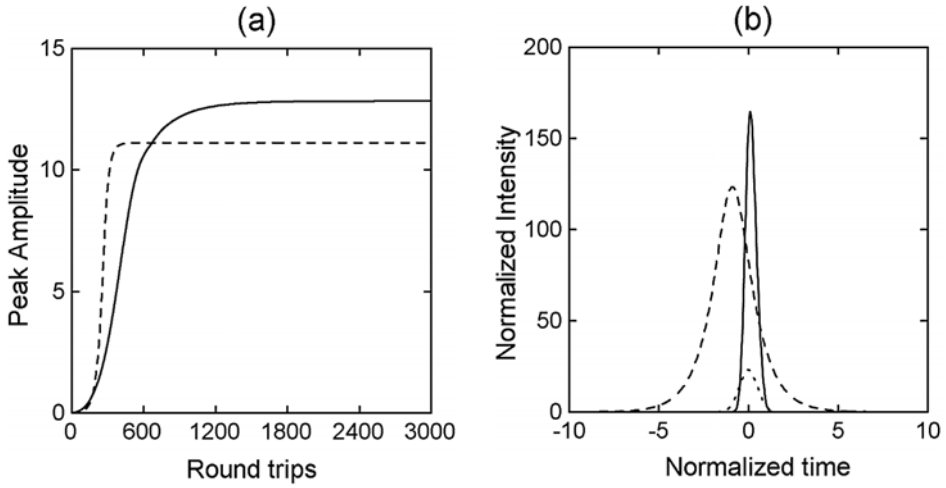

Fig. 8 – (a) Output peak-amplitude as a function of round trip number of the solitary-wave formed by alternatively keeping in resonator the wave corresponding to point C in Fig. 1(b) ($\lambda = 1.198$ μm, $t = 165°C$) (solid line), and the wave corresponding to point E in Fig. 1(b) ($\lambda = 2.079$ μm, $t = 165°C$) (dashed line). The pump intensity is in both cases $I_p = 0.8$ GW/cm^2 and the refectivity is asummed to be $R = 0.982$. (b) The corresponding output intensity profile. With dotted line we have represented the input pump.

In all our numerical runs we have included the third-order self-phase modulation effect for the signal wave. We have also checked whether this effect is of great importance for solitary-wave formation. Fig. 9 shows comparatively the result of two simulations with and without taking into account the cubic nonlinearity for the signal wave. As one should expect, the presence of cubic nonlinearity leads to a more focused and intense signal wave. The results presented in Fig. 9(a) show that the signal buil-up time is practically the same in both cases.

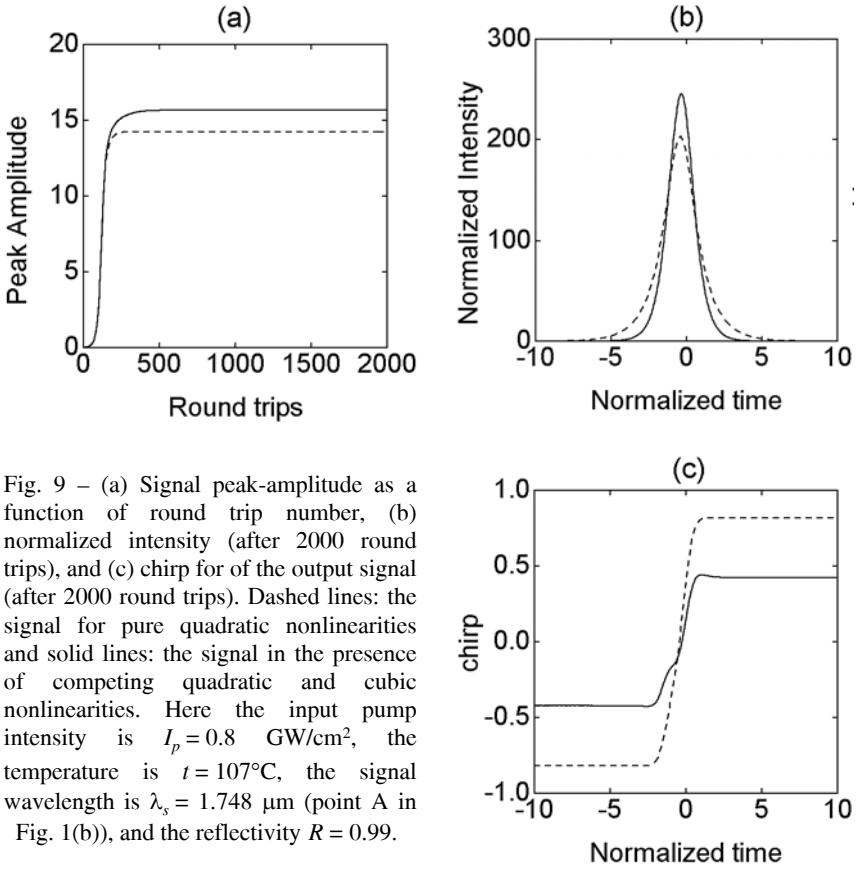

Fig. 9 – (a) Signal peak-amplitude as a function of round trip number, (b) normalized intensity (after 2000 round trips), and (c) chirp for of the output signal (after 2000 round trips). Dashed lines: the signal for pure quadratic nonlinearities and solid lines: the signal in the presence of competing quadratic and cubic nonlinearities. Here the input pump intensity is $I_p = 0.8$ GW/cm^2, the temperature is $t = 107$°C, the signal wavelength is $\lambda_s = 1.748$ μm (point A in Fig. 1(b)), and the reflectivity $R = 0.99$.

In order to better characterize the signal formed in these two cases we have represented in Fig. 9(c) the chirp of the emerging signal. Notice that, in the case of pure qudratic nonlinearities, the chirp displays a smoother behavior as compared to the case of competing quadratic and cubic nonlinearities.

Another important parameter in a singly resonant OPO is the crystal length L. By varying the crystal length, at a given pumping rate, we have observed enormous differences in the shape of the formed signal. We have observed that, when pumping the cavity with 1 ps pump pulses and $I_p = 0.4$ GW/cm^2, if the crystal length exceeds a critical value, which for the above parameters was found to be between 8.5 mm and 9 mm, the resonated signal splits into a train of pulses, each of them being about 10 times shorter than the input pump pulse (see Fig. 10). Contrary to the case of smoother sigal pulses (obtained for crystals shorter than the critical length), these pulse trains are no more stationary.

Fig. 11 shows the output signal intensity for various pump irradiances when using 300 fs pump pulses and a crystal with $L = 2.5$ mm. One can see that, for sufficiently large pump intensities, the emerging signal profile displays pronounced

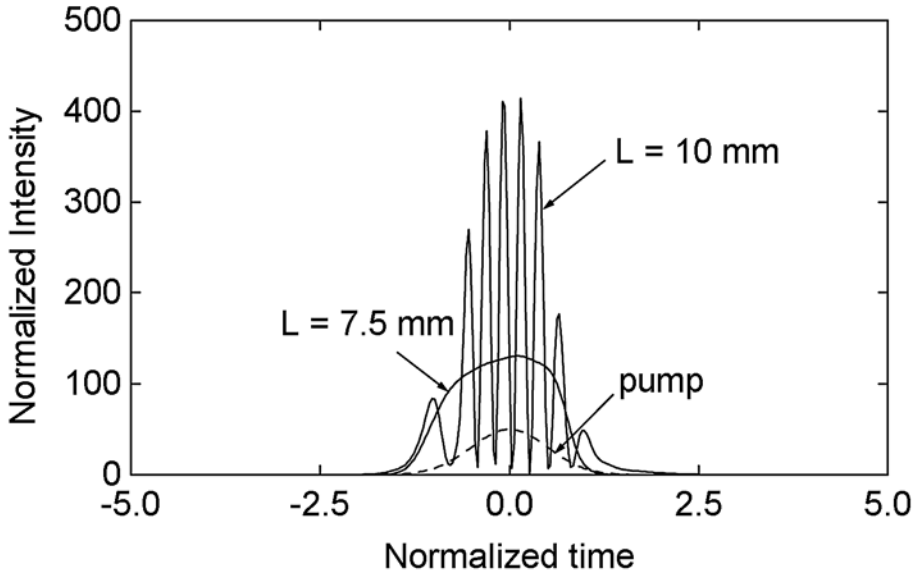

Fig. 10 – Intensity profile of the emerging signal for two different crystal lengths indicated with the arrows. The parameters correspond to point A in Fig. 1(b) and the reflectivity is $R = 0.96$. The intensity of the 1 ps pump pulse is $I_p = 0.4$ GW/cm^2.

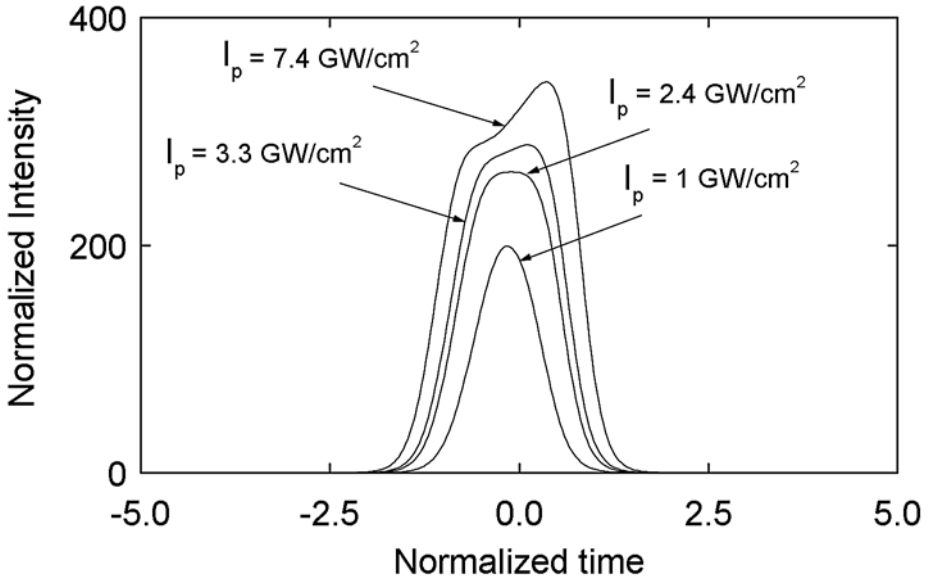

Fig. 11 – Intensity profile of the emerging signal for four different pump intensities indicated with the arrows. The parameters correspond to point A in Fig. 1(b), the reflectivity is $R = 0.96$, the pump duration is 300 fs and the crystal length is $L = 2.5$ mm.

"shoulders". For huge pump intensities a stationary regime for the resonated wave cannot be achieved and the shape of the signal wave displays a multipeaked structure.

The influence of the time delay between the fresh pump and the signal on the solitary wave formation was also investigated. Our simulations show that the solitary wave no more forms if we deteriorate the synchronization (a 10 fs time delay is very harmful for 300 fs pump pulses with $I_p = 0.4$ GW/cm^2). However, for moderate time delays we have observed the formation of stationary solitary waves (see Fig. 12).

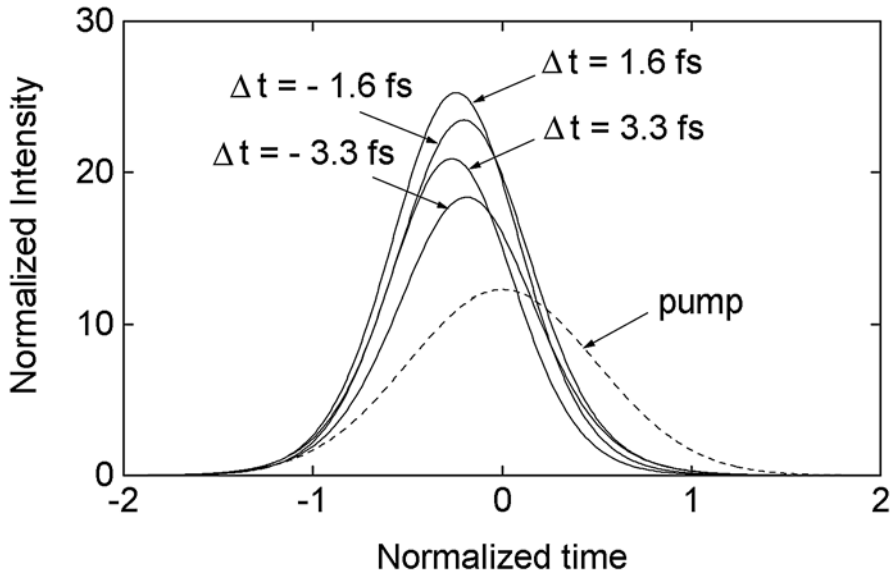

Fig. 12 – Signal intensity profile for various desynchronizations Δt between pump and signal waves. The parameters correspond to point A in Fig. 1(b), the reflectivity is $R = 0.96$, the pump duration is 300 fs, the pump intensity is $I_p = 0.4$ GW/cm^2 and $L = 2.5$ mm.

4. CONCLUSIONS

We have numerically investigated the possibility of solitary wave formation in a synchronously pumped singly resonant lithium triborate-based optical parametric oscillator for pump pulses lengths from femtosecond to picosecond domain. For a large domain in the femtosecond regime the solitary waves formed obey a *pump amplitude* × *signal width* = *constant* law. A high (up to 5-fold) pulse compression may be achieved, when the parametric device operates in the picosecond regime. Stationary pulse propagation regimes are shown to occur also for small anomalous and normal dispersions at the resonated frequency. The crystal length was shown to

be an important parameter determining, when exceeding a critical value, the splitting of the signal pulse into a train of very short pulses. The desynchronization parameter plays also an important role in the solitary wave formation process. By increasing the time delay between pump and signal the solitary wave formation is suppressed. The present analysis emphasizes the remarkable properties of the lithium triborate crystal. If one takes diffractive effects into account it can be anticipated that stationary spatiotemporal solitons ("light bullets") (see, *e.g.*, [35, 36] and the references cited therein) may be formed in this type of singly resonant optical parametric oscillator.

REFERENCES

1. M. H. Dunn and M. Ebrahimzadeh, Science, **286**, 1513 (1999).
2. M. Ebrahimzadeh, R. C. Eckardt and M. H. Dunn, eds., Special issue on *Optical parametric devices and processes*, J. Opt. Soc. Am., B **16**, 1477 (1999).
3. W. R. Bosenberg and R. C. Eckardt, eds., Special issue on *Optical parametric devices*, J. Opt. Soc. Am., B **12**, 2083 (1995).
4. R. L. Byer and A. Piskarskas, eds., Special issue on *Optical parametric oscillation and amplification*, J. Opt. Soc. Am., B **10**, 1655 (1993).
5. K. I. Martin, W. A. Clarkson, and D. C. Hanna, Appl. Opt., **36**, 4149 (1997).
6. S. Schiller and J. Mlynek, eds., Special issue on *Continuous-wave optical parametric oscillators: materials, devices and applications*, Appl. Phys., B **66**, 663 (1998).
7. M. Ebrahimzadeh, G. A. Turnbull, T. J. Edwards, D. J. M. Stothard, I. D. Lindsay, and M. H. Dunn, J. Opt. Soc. Am., B **16**, 1499 (1999).
8. G. D. Miller, R. G. Batchko, W. M. Tulloch, D. R. Weise, and M. M. Fejer, R. L. Byer, Opt. Lett., **22**, 1834 (1997).
9. U. Strössner, A. Peters, J. Mlynek, S. Schiller, J. P. Meyn, and R. Wallenstein, Opt. Lett., **24**, 1602 (1999).
10. D. R. Weise, U. Strössner, A. Peters, J. Mlynek, S. Schiller, A. Arie, A. Skliar, and G. Rosenman, Opt. Commun., **184**, 329 (2000).
11. C. McGowan, D. T. Reid, Z. E. Penman, M. Ebrahimzadeh, W. Sibbett, and D. H. Jundt, J. Opt. Soc. Am., B **15**, 694 (1998).
12. P. Loza-Alvarez, D. T. Reid, P. Faller, M. Ebrahimzadeh, and W. Sibbett, J. Opt. Soc. Am., B **16**, 1553 (1999).
13. L. Lefort, K. Puech, S. D. Butterworth, Y. P. Svirko, and D. C. Hanna, Opt. Lett., **24**, 28 (1999).
14. T. J. Edwards, G. A. Turnbull, M. H. Dunn, and M. Ebrahimzadeh, Opt. Express, **6**, 58 (2000).
15. P. Loza-Alvarez, D. T. Reid, P. Faller, M. Ebrahimzadeh, W. Sibbett, H. Karlsson, and F. Laurell, Opt. Lett., **24**, 1071 (1999).
16. J. D. V. Khaydarov, J. H. Andrews, and K. D. Singer, Opt. Lett., 19 (1994) 831.
17. J. D. V. Khaydarov, J. H. Andrews, and K. D. Singer, J. Opt. Soc. Am., B **12**, 2199 (1995).
18. E. Ibragimov, A. A. Struthers, D. J. Kaup, J. D. Khaydarov, and K. D. Singer, Phys. Rev., E **59**, 6122 (1999).
19. A. Umbrasas, J.-C. Diels, J. Jacob, and A. Piskarskas, Opt. Lett., **19**, 1753 (1994).
20. C. Rauscher, T. Roth, R. Laenen, and A. Laubereau, Opt. Lett., **20**, 2003 (1995).
21. G. M. Gale, M. Cavallari, and F. Hache, J. Opt. Soc. Am., B **15**, 702 (1998).
22. M. Ghotbi and M. Ebrahim-Zadeh, Opt. Express, **12**, 6002 (2004).
23. D. T. Reid, J. M. Dudley, M. Ebrahimzadeh, and W. Sibbett, Opt. Lett., **19**, 825 (1994).

24. P.-S. Jian, W. E. Torruellas, M. Haelterman, S. Trillo, U. Peschel, and F. Lederer, Opt. Lett., **24**, 400 (1999).
25. S. Lin, J. Y. Huang, J. Ling, C. Chen, and Y. R. Shen, Appl. Phys. Lett., **59**, 2805 (1991).
26. Z. Xu, X. Liu, D. Deng, Q. Wu, L. Wu, B. Wu, S. Lin, B. Lin, C. Chen, and P. Wang, J. Opt. Soc. Am., B **12**, 2222 (1995).
27. M. Ebrahimzadeh, S. French, and A. Miller, J. Opt. Soc. Am., B **12**, 2180 (1995).
28. J. Y. Zhang, J. Y. Huang, Y. R. Shen, and C. Chen, J. Opt. Soc. Am., B **10**, 1758 (1993).
29. B. Wu, F. Xie, C. Chen, D. Deng,and Z. Xu, Opt. Commun., **88**, 451 (1992).
30. Y. Tang, Y. Cui, M. H. Dunn, J. Opt. Soc. Am., B **12**, 638 (1995).
31. S. D. Butterworth, S. Girard and D. C. Hanna, J. Opt. Soc. Am., B **12**, 2158 (1995).
32. T. W. Tukker, C. Otto, and J. Greve, Opt. Commun., **154**, 83 (1998).
33. B. Ruffing, A. Nebel, and R. Wallenstein, Appl. Phys., B **72**, 137 (2001).
34. A. Agnessi, G. C. Reali, V. Kubecek, S. Kamazaki, Y. Takagi, and K. Yoshibara, J. Opt. Soc. Am., B **10**, 2211 (1993).
35. D. Mihalache, D. Mazilu, L.-C. Crasovan, L. Torner, B. A. Malomed, and F. Lederer, Phys. Rev., E **62**, 7340 (2000).
36. B. A. Malomed, D. Mihalache, F. Wise, and L. Torner, J. Opt. B: Quantum Semiclass. Opt., **7**, R53 (2005).